Downstream and In-situ: Two Perspectives on Initiation of Monsoon Low Pressure Systems over Bay of Bengal

A Thesis

submitted to

Indian Institute of Science Education and Research, Pune

Department of Earth and Climate Science

in partial fulfilment of the requirements for the

BS MS Dual Degree Programme

by

Meera Mohan

Indian Institute of Science Education and Research, Pune

Dr. Homi Bhabha Road,

Pashan, Pune, 411008, INDIA

Supervisor : Dr. Suhas Ettammal

April 2019

Certificate

This is to certify that this dissertation entitled ***"Downstream and In-situ: Two Perspectives on Initiation of Monsoon Low Pressure Systems over Bay of Bengal"*** towards the partial fulfilment of the BSMS dual degree programme at the Indian Institute of Science Education and Research, Pune, represents study/work carried out by Meera Mohan at Indian Institute of Science Education and Research, Pune, under the supervision of Dr. Suhas Ettammal, Assistant Professor, Department of Earth and Climate Science, during the academic year 2018-2019.

Dr. Suhas Ettammal

Meera Mohan

Declaration

I hereby declare that the research work presented in the report entitled ***"Downstream and In-situ: Two Perspectives on Initiation of Monsoon Low Pressure Systems over Bay of Bengal"*** have been carried out by me at the Department of Earth and Climate Science, Indian Institute of Science Education and Research, Pune, under the supervision of Dr. Suhas Ettammal and the same has not been submitted elsewhere for any other degree.

Dr. Suhas Ettammal

Meera Mohan

ACKNOWLEDGEMENTS

I would like to thank my supervisor, Dr. Suhas Ettammal, for his guidance and for being patient with me throughout the course of the project. I would also like to thank my thesis advisor, Dr. Neena Joseph Mani, for her invaluable comments and suggestions regarding the project. I express my sincere gratitude to my parents and friends for being a constant source of support and encouragement. I am extremely grateful to IISER Pune for providing me with this year-long opportunity to pursue a research problem.

CONTENTS

LIST OF FIGURES iii

LIST OF TABLES v

1. INTRODUCTION 2

2. DATA AND METHODS 8

3. RESULTS 13

3.1. Statistics of low pressure system initiation 13

3.2. Composite structure 19

3.2.1. In-situ propagating composite 19

3.2.2. Downstream composite 24

4. DISCUSSION 29

5. CONCLUSION 31

REFERENCES 32

LIST OF FIGURES

Figure 1: Locations of initiation of low pressure systems (downstream, *in-situ* westward propagationg, *in-situ* eastward propagating and *in-situ* non propagating events) during monsoon for 1979 to 2019 13

Figure 2: Monthly variation in low pressure initiation (downstream, *in-situ* westward propagationg, *in-situ* eastward propagating and *in-situ* non propagating events) for 1979 to 2017 over Bay of Bengal 14

Figure 3: Composite plots of relative vorticity anomaly (in 10^{-5} s^{-1}) at 850 hPa for (a) downstream (b) *in-situ* propagating (c) *in-situ* non-propagating and (d) *in-situ* eastward propagating events. Count represents the number of events of each type with their respective percentages (of the total) in brackets. 16

Figure 4: Mean track of (a) *in-situ* westward propagating and (b) downstream events with their respective most probable paths 17

Figure 5: Inter annual variability in LPS (*in-situ* , downstream and total number of events) initiation. The lines drawn without markers indicate the trend in the time series. 18

Figure 6: Lifecycle composite of *in-situ* propagating events for (a) t_0 - 4 (b) t_0 - 2 (c) t_0 (d) t_0 + 2 and (e) t_0 + 4, where t_0 is the initiation date. Shading denotes vorticity anomaly (in 10^{-5} s^{-1}) at 850 hPa, black contours denote surface pressure anomaly (in hPa) and the arrows represent the horizontal winds (in m s^{-1}) at 1000 hPa. Reference wind vector has magnitude of 15 m s^{-1}. 20

Figure 7: Relative vorticity anomaly composite (a) zonal cross section of vertical profile centred at the latitude of low (b) horizontal structure at 850 hPa with wind vectors of *in-situ* propagating events. Shading denotes vorticity anomaly (in 10^{-5} s^{-1}), arrows represent the horizontal wind anomaly (in m s-1) at 850 hPa. Reference wind vector has magnitude of 10 m s^{-1} 21

Figure 8: (a) Meridional cross section of zonal velocity profile (b) Zonal cross section of meridional velocity of *in-situ* propagating events. Dashed contours indicate negative values. Units are in m s^{-1}. 22

Figure 9: (a) Zonal cross section of pressure velocity anomaly profile (in 10^{-2} Pa s^{-1}) (b) Meridional cross section of Potential Vorticity anomaly profile (in 10^{-7} K m^2 kg^{-1} s^{-1})

(c) Meridional cross section of temperature anomaly profile (in K) (d) zonal cross section of specific humidity anomaly profile (in g/kg) of in-situ propagating events 23

Figure 10: Lifecycle composite of downstream events for (a) t_0 - 4 (b) t_0 - 2 (c) t_0 (d) t_0 + 2 and (e) t_0 + 4, where t_0 is the initiation date. Shading denotes vorticity anomaly (in 10^{-5} s^{-1}) at 850 hPa, black contours denote surface pressure anomaly and the arrows represent the horizontal winds (in m s^{-1}) at 1000 hPa. Reference wind vector has magnitude of 15 m s^{-1}. 25

Figure 11: Relative vorticity anomaly composite (a) zonal cross section of vertical profile centred at the latitude of low (b) horizontal structure at 850 hPa with wind vectors of downstream events. Shading denotes vorticity anomaly (in 10^{-5} s^{-1}), arrows represent the horizontal wind (in m s^{-1}) at 850 hPa. Reference vector has magnitude of 10 m s^{-1}. ... 26

Figure 12: (a) Meridional cross section of zonal velocity profile (b) Zonal cross section of meridional velocity of downstream events. Dashed contours indicate negative values. Units are in m s^{-1} 27

Figure 13: (a) Zonal cross section of pressure velocity anomaly profile (in 10^{-2} Pa s^{-1}) (b) Meridional cross section of Potential Vorticity anomaly profile (in 10^{-7} K m^2 kg^{-1} s^{-1}) (c) Meridional cross section of temperature anomaly profile (in K) (d) zonal cross section of specific humidity anomaly profile (in g/kg) of downstream events 28

LIST OF TABLES

Table 1 : Initiation dates (in dd/mm/yyyy) of (a) *in-situ* westward propagating (b) *in-situ* eastward propagating (c) *in-situ* non propagating and (d) downstream events for 1979 to 2017 10

Table 2 : Classification of monsoon LPS using sea level pressure anomaly and maxima of horizontal wind at the surface based on IMD criteria 12

ABSTRACT

Monsoon low pressure systems (LPS) contribute to nearly half of the total summer monsoon rainfall over central India. As their mechanism is not well understood, their contribution is ill-represented in climate models, which has led to the underestimation of rainfall over central India in simulations. The initiation of these systems is commonly considered to be produced by atmospheric instabilities that grow in time and space. The influence of western Pacific typhoons in generating lows over Bay of Bengal has been overlooked in most of the studies. Their influence, termed as downstream amplification, contributes to 32% of the total, in comparison to the 68% by *in-situ* processes, obtained by examining 256 cases of LPS initiation from 1979 to 2017. This is in contrast to the results of some of the previous studies that attribute the majority of LPS initiation to downstream processes. Composite structures reveal that *in-situ* and downstream generated events essentially represent the same physical system, having similar dynamic and thermodynamic features, but differing in their mode of initiation. Lows initiated *in-situ* display greater randomness in the initiation date and location compared to downstream events that are preferentially initiated east of the head Bay, mainly in the months of August and September. The declining trend seen in the downstream generated cases suggests that the prediction of the initiation of LPS will become increasingly difficult in the future. Influence of vertically propagating Potential Vorticity (PV) anomalies and intensification of LPS over land are some of the factors that need to be explored.

1. INTRODUCTION

Monsoon is an atmosphere-ocean coupled phenomenon which regularly transports moisture from the ocean to the continents. The Asian monsoon system acts as an inter-hemispheric solar collector, with the Tibetan plateau being a source of heat and region of low pressure during the northern hemispheric summer season, towards which the moisture-laden south-westerly winds flow (Webster and Fasullo, 2003). In comparison to the various monsoon systems in the world, the Asian monsoon is distinct in its land-ocean configuration, the Himalayan topography acting as a barrier, the presence of horizontal and vertical shear of the zonal wind and the Inter Tropical Convergence Zone (ITCZ) performing as virtual topography to produce rainfall over the plains of central India.

The monsoon circulation system is composed of various scales of motion. The intraseasonal scale (30-60 day), synoptic scale (2-10 day), mesoscale processes, to name a few, interact with each other, organise convection and modify the finer features of monsoon. Of these, the monsoon low pressure systems (LPS) contribute to nearly half of the summer monsoon rainfall over the central Indian region (Yoon and Chen, 2005). These are cyclonic, convectively coupled systems, forming mostly over the Bay of Bengal in a monsoon background environment and typically propagate north-westward against the mean flow, along the monsoon trough, into land. Based on the surface wind, pressure and relative vorticity field values, the India Meteorological Department (IMD) classified these disturbances into lows, depressions, deep depressions and cyclones (Refer Table 2). An average of 6 depressions and 8 lows form during the monsoon season (IMD Monsoon Report, 2018).

One of the most studied LPS is the monsoon depression (MD). It is a synoptic scale disturbance that has a horizontal spatial scale of ~2000 km and a temporal scale of 2-5 days. The initial studies of the system were case studies which explored the structure of a MD. According to one such study by Sikka in 1978, the MDs have highest cyclonic vorticity in the lower troposphere which remains cyclonic up to 250 hPa, a warm core over cold core temperature structure and highest rainfall associated with the system occurring in a region southwest of the depression centre. Bay of Bengal is an ideal environment for these systems to develop in terms of the warm sea surface temperatures, the high vorticity provided by the monsoon trough and large-scale

curvature of the monsoonal flow present in the region (Sikka, 1978). The composite structure of MDs in different geographical locations reveal that the Indian MDs are similar in terms of their dynamic and thermodynamic structure to those that form in the western Pacific and northern Australia (Hurley and Boos, 2014).

The earliest studies approximated the dynamics of the system using Quasi Geostrophic (QG) equations (Shukla, 1978; Sanders, 1984). Rossby number (Ro) is a parameter that quantifies the effect of rotation imparted by the dynamical fields in comparison to the rotation of earth. For the QG assumptions to be valid, Rossby number, formulated to be a parameter which compares the magnitudes of the influence of ageostrophic circulations to the theoretical geostrophic circulations, has to be less than one. It has proved to be ineffective in the tropical region during the monsoons (Ro >1) due to the presence of strong ageostrophic circulations (Boos et al., 2014). The role of boundary layer in providing moisture and the frictional convergence which helps in spinning up the vortex is ignored in the quasi-geostrophic framework. The set of quasi-geostrophic equations become insufficient to account for all the state variables including moisture. In recent works, potential vorticity (PV), which combines both dynamic and thermodynamic fields, has emerged as a parameter to study monsoon depressions (Boos et al., 2014). Monsoon depressions are conceived as columns of PV extending from the surface to upper troposphere with a bimodal distribution of maximum values (Boos et al., 2014; Hunt et al., 2016).

Majority of the studies concerning MDs resort to a linear perturbation analysis of the system. This limits the interaction among the scales of motion present during monsoon. In addition, the analysis done by Diaz and Boos (2019), showed that the spatial scales of the mean flow and MDs were comparable, raising questions about the validity of scale separation.

The importance of background flow has been neglected in several numerical model simulations. It is either treated as a constant or set to zero. The study on MD by Shukla (1976), with a 10 layer model using the QG system of equations show that the scales that display the highest growth rates correspond to the smallest scales, i.e., the convective scales in the absence of a background flow. Diaz and Boos (2019) explore the response of the atmosphere with and without the presence of a constant zonally varying monsoonal background flow. In the absence of background, the propagation

speed, direction, amplitude and the horizontal scale (corresponding to mesoscale disturbances), are considerably different from that of observations, whereas the application of background helps to capture most of these features. The analysis highlights the role of background flow in scale selection.

In a recent study (Diaz and Boos, 2019), an examination of the contribution of various terms to the generation of perturbation kinetic energy with heating impulse concentrated at different locations shows that the growth by horizontal shear of the mean zonal flow has a preferred location near the head Bay, where the track density of MDs is found to be high. This in a way explains why the region is a preferred location for LPS initiation.

Monsoon depressions are considered as phenomena influenced mainly by the dynamics of atmosphere. The ocean is regarded as merely a source of moisture. Most of the theoretical models that deal with the initiation of lows attribute their initiation to some form of atmospheric instability. The contribution of wave disturbances from the Pacific in providing moisture, momentum and energy is not considered. A source of rotation is important for the formation of MDs in the tropical region where planetary vorticity is low. Some of the previous studies list two ways in which a low is initiated: *in-situ* over Bay of Bengal and by downstream amplification (Krishnamurti et al., 1977; Saha et al., 1981).

In the monsoon environment, a favourable background with high rotation is provided by the Inter Tropical Convergence Zone (ITCZ), a region of strong, organised convection and converging monsoonal winds which helps in the *in-situ* development of lows. Propagating disturbances originating in the Pacific, with high rotational component of the winds, can transport momentum westward and initiate lows by downstream amplification. The tropical atmosphere is conditionally unstable (Williams and Renno, 1993). By the parcel model, if there exists some kind of lifting mechanism, provided either by the propagating disturbances from the Pacific or by the atmospheric instability, convective available potential energy (CAPE) can be accessed.

The models do not represent the convectively coupled nature of these systems, where circulation and convection fields modify each other. The forcing applied is either of constant magnitude (Goswami, 1987) or present only in the initial stages as a heating impulse (Diaz and Boos, 2019). The heating used in studies often has the structure of

the first baroclinic mode, with maxima in the middle levels. The effects of various types of clouds, namely, their heating profiles or radiative cooling is not accounted for. Shukla (1976) used different heating profiles in his model and found that the horizontal scale selection depends on the vertical extent of heating.

The role of moisture and its variation in time and space has largely been ignored in theoretical studies of the LPS. The moisture fields are modified by dynamical fields through advection and evaporation. The thermodynamic equation connects the dynamic and moisture fields. The release of latent heat of condensation acts as forcing for the dynamical fields, which further modifies them. A non-linear behaviour appears to be imparted to the system with the addition of moisture. In a recent study by Adames and Ming (2018), a prognostic moisture equation is used. They use a budget analysis of moisture and horizontal distribution of terms in the budget to show that the vertical advection of moisture and precipitation are important processes in the maintenance and propagation of moisture anomalies. Their model accounts for the presence of a moving heat source whose magnitude is modified (dependent on the dynamical fields) during the propagation of the system.

Barotropic, baroclinic instability mechanisms and their numerous modifications are unable to represent the intensification of MDs (e.g. Sanders, 1984). Even though the structures look similar, their growth rate is considerably reduced. Various mechanisms could work in tandem to help the growth and maintenance of the LPS. A single mechanism may not be able to explain all the observed features.

Propagation mechanisms that have been suggested include those based on simple considerations of a moving heat source with constant magnitude (Goswami, 1987), using linearized shallow water equations. The model predicts maximum rainfall to the north-west of the centre of the system which contradicts the observation of maximum precipitation in the south-western sector. Also, the heating produces a Rossby wave response in the atmosphere which has a temporal scale of the quasi-biweekly or 14-day mode (Chatterjee and Goswami, 2004), different from that of MDs. Quasi geostrophic considerations attribute vortex stretching mechanism to the propagation of the system. Through a vorticity budget, Boos et al. (2014) show that the horizontal distribution of the vortex stretching term is such that it would cause the system to move south-westwards, as opposed to their north-westward movement. Other mechanisms

suggested include an approach based on the movement of PV maximum by adiabatic drift (Boos et al., 2014) and the interaction of vortices with the Himalayas which act as a boundary (Hunt and Parker, 2016).

Spectral analysis of the distribution of power for the field variables (after isolating the spatial and temporal scales corresponding to LPS) associated with monsoon LPS in the frequency-wavenumber domain shows that it does not correspond to any of the theoretical modes selected by the shallow water model. This may be considered as evidence for their coupling with convection and they are called as moist modes. Their scales correspond to those of Tropical Depression-type waves, identified as one of the convectively coupled equatorial wave modes by Roundy and Frank (2004); Kiladis et al. (2009).

In 2018, various parts of the country experienced high anomalous rainfall and floods around which time low pressure systems were active in the Bay of Bengal (IMD Report, 2018). The neighbouring western Pacific region had high cyclonic activity during this period. Two of the MDs intensified into cyclones, one that hit the Odisha coast in September and another in October. In both cases, typhoons occurred in the Pacific few days prior to the formation of LPS over Bay of Bengal.

Krishnamurti et al. (1977) found 35 cases of downstream amplification in 43 years (1933-1976) of daily pressure anomaly data. The statistics quoted by Saha et al. (1981) attributes 87% (45 out of 52) of low pressure initiation to downstream amplification during the 10 year period from 1969-1978, based on 24-hour change in sea level pressure. Both of these studies suggest that a significant percentage of lows are initiated by downstream amplification. Still, these processes were not accounted for in the numerous theoretical models that followed, where the focus was on representing the system as a growing atmospheric instability, generated *in-situ*. The mechanisms for the initiation and growth of LPS are not well understood, which has led to the systematic underestimation of summer monsoon rainfall over central India in many model simulations.

In this context, it is important to understand the formation, propagation and the processes that help to sustain these low pressure systems. Dealing with the system in its full complexity is difficult due to the highly non-linear nature of the interaction between various scales.

We try to examine the behaviour of the system with reference to how LPS are initiated. Different physical processes may be important for selecting these systems to be one of the preferred scales of motion during the summer monsoon season. To simplify the study, the lows are categorised into *in-situ* and downstream generated cases. As they are initiated by different physical processes, we inspect the cases closely to determine if they are dynamically different systems or not.

The main objectives of this study are:

- *To examine the contribution of the two different physical processes to initiation of lows over Bay of Bengal;*
- *To extract the statistics of LPS initiation to quantify the effect of the influence of disturbances from the Western Pacific;*
- *To identify the locations of initiation of low pressure systems and check if the two categories differ in terms of their initiation location;*
- *To derive a composite structure for each category and compare their dynamic and thermodynamic fields to verify the physical validity of this classification.*

In Chapter 2, we describe the dataset used for the study and outline the procedures applied for performing the analysis. The tracking algorithm used to calculate the composite structure is also defined. The next chapter includes a description of the results. The statistics of low initiation is extracted to account for the contribution of each of the physical process. The category of initiation is inferred from the time-longitude distribution of relative vorticity anomaly maps at 850 hPa and their characteristics are noted. The location and the monthly variation in low initiation are also examined. A composite Eulerian (field view) and Lagrangian view (by tracking along the system) of the LPS is presented for each category to identify their common features and to distinguish between them. The results are summarised and the implications discussed in Chapter 4. The final chapter concludes the main findings of the study.

2. DATA AND METHODS

ERA Interim reanalysis data which is available four times daily (6 hourly data) with $0.75^{o} \times 0.75^{o}$ horizontal resolution and vertical resolution of 25 levels between 1000 hPa and 150 hPa, for 39 years, from 1979 to 2017 is used for the study (*ERA Interim, Daily. ECMWF | Public Datasets. http://apps.ecmwf.int/ datasets/data/ interim-full-daily/levtype=sfc/*). Vertical component of relative vorticity, potential vorticity, specific humidity, surface pressure, temperature, vertical pressure velocity, zonal and meridional wind are the variables analysed. Only the cases of LPS initiation occurring in the monsoon season (June, July, August, and September) are considered for the analysis.

Identification of LPS initiation dates over Bay of Bengal (from 1979 to 2003) and their position is aided by the data compiled by Sikka (2006) and for the remaining years (2004 to 2017) by Praveen et al. (2015). The Sikka archive uses daily surface pressure charts of IMD for identification of initiation dates. The detection of lows is done manually based on the presence of closed pressure contours at 2 hPa interval in the charts. The second dataset uses an automated algorithm to detect and track LPS by locating minima in sea level pressure.

In this study, we regard LPS as perturbations on a mean monsoonal state. Their influence is analysed by removing the effects of the mean, i.e., by removing climatology from the total field. A four-times daily climatology is created for the relative vorticity field and the anomaly (from this climatology) is calculated. The initiation of a low pressure system is attributed to either *in-situ* processes or the influence of propagating wave disturbances from the Pacific which are explored in the relative vorticity anomaly distribution.

From the time-longitude distribution (Hovmoller diagram) of the relative vorticity anomaly at 850 hPa (obtained after averaging across the latitude range of the event), the process of downstream propagation is identified by the presence of a region that shows positive anomaly values with a westward slope extending from the longitudes of western Pacific to those corresponding to Bay of Bengal. *In-situ* cases are further classified into westward, eastward and non-propagating events. The number of downstream and *in-situ* cases occurring in each year and their location of initiation is

noted. As the identification is based on subjective analyses, there could be errors in the classification. Averaging over many events is expected to overcome the shortcomings of the procedure.

Table 1 lists the initiation dates of in-situ westward propagating, non-propagating, eastward propagating and downstream events.

Table 1a: Initiation dates of in-situ westward propagating events

In-situ westward propagating events (dd/mm/yyyy)					
21/06/1979 28/09/1979	14/09/1980	19/06/1981 07/08/1981 21/09/1981 26/09/1981	04/06/1982 20/07/1982 10/08/1982 16/08/1982	10/07/1983 17/08/1983 22/09/1983	13/06/1984 30/07/1984 05/08/1984 11/09/1984
30/07/1985 30/09/1985	18/08/1986	16/08/1987	18/07/1988 22/09/1988 2/10/1988	11/06/1989 26/06/1989 17/07/1989 18/08/1989 23/08/1989 25/09/1989	13/06/1990 15/08/1990 20/08/1990
04/06/1991 11/08/1991	16/06/1992 01/08/1992 23/09/1992	31/07/1993	03/07/1994 24/08/1994	31/08/1995 26/09/1995	12/06/1996 15/06/1996 27/09/1996
15/06/1998 29/07/1998	06/06/2000 07/08/2000 17/08/2000 23/08/2000	11/08/2001 01/10/2001	16/07/2002 31/07/2002 06/08/2002 21/08/2002	04/08/2003	12/06/2004 02/07/2004 14/07/2004 02/08/2004 20/08/2004 21/09/2004
01/06/2005 24/07/2005 05/09/2005 18/09/2005	28/06/2006 06/09/2006 18/09/2006	30/05/2007 24/06/2007 24/06/2007 27/06/2007 11/07/2007	14/06/2008 07/07/2008 30/07/2008 14/09/2008 12/09/2008	17/06/2009 30/08/2009 24/08/2009 03/09/2009 26/09/2009	09/06/2010 04/08/2010 07/09/2010
13/06/2011 27/08/2011 30/08/2011	19/07/2012 03/08/2012	13/06/2013 22/06/2013 21/07/2013 17/08/2013	12/07/2014 27/07/2014 15/09/2014	21/06/2015 31/07/2015 15/09/2015	17/06/2016 27/06/2016 10/07/2016 25/08/2016 05/09/2016 23/09/2016
24/06/2017 19/08/2017					

Table 1b: Initiation dates of in-situ eastward propagating events

In-situ eastward propagating events (dd/mm/yyyy)					
03/06/1980	15/06/1982 27/09/1982	20/06/1984	10/06/1987	30/08/1996	08/08/2002
07/06/2005	03/09/2007	04/06/2015			

Table 1c: Initiation dates of in-situ non propagating events

In-situ non propagating events (dd/mm/yyyy)					
10/09/1979 20/09/1979 11/08/1979	03/10/1980 15/06/1980	08/06/1981 30/08/1981	14/09/1983 28/09/1983 26/06/1983	31/05/1984 31/08/1984	04/06/1987
19/06/1989	19/06/1990	15/09/1991	06/09/1992	14/06/1993 05/09/1993	15/09/1994
12/07/1995	06/09/1996 09/08/1996	23/06/1997	07/09/1998 02/07/1998	27/08/1999 11/09/1999	11/06/2001 09/08/2001
20/06/2002 22/09/2002	22/07/2003 30/07/2003 05/09/2003	13/09/2004	11/08/2005	23/09/2008	20/08/2010 10/09/2010 27/09/2010
18/09/2012	20/09/2013	02/08/2014	03/07/2015 27/07/2015	11/06/2017 30/09/2017	

Table 1d: Initiation dates of downstream events

Downstream events (dd/mm/yyyy)					
02/07/1979 04/08/1979	28/06/1980 04/07/1980 21/07/1980 20/08/1980 24/08/1980 31/08/1980	06/07/1981 05/08/1981 11/08/1981	30/07/1982 10/08/1982 26/08/1982 04/09/1982	19/07/1983 03/09/1983	16/07/1984 11/08/1984
04/08/1985 12/08/1985 08/09/1985 19/09/1985	06/08/1986 27/08/1986 08/09/1986 22/09/1986	23/08/1987	06/08/1988 18/09/1988	22/07/1989 10/08/1989 28/08/1989 10/09/1989	10/09/1990 18/09/1990
15/07/1991 20/07/1991 25/07/1991 27/08/1991	16/07/1992	08/08/1993 22/09/1993	18/09/1996 29/07/1996	02/08/1997 25/08/1997	15/06/1999 31/07/1999 05/08/1999
06/07/2001	21/08/2003 25/08/2003 11/09/2003	26/07/2004 10/09/2004	31/07/2006 10/08/2006 20/08/2006 27/08/2006	12/09/2007	08/08/2008
12/07/2009 18/07/2009 24/07/2009	17/09/2010	13/09/2011 19/09/2011	09/06/2012 02/09/2012	04/08/2013 16/09/2013 28/09/2013	20/07/2014 31/08/2014 04/09/2014 19/09/2014
18/09/2015	30/07/2016 16/08/2016 21/08/2016	27/08/2017 17/09/2017			

To study the propagation character of lows, a composite picture is created by averaging across the corresponding latitudes of events and then across all the events in a category. This helps in obtaining the common character of events, even though they occur at different times and locations. The choice of latitudes for averaging takes into account the meridional motion and the meridional extent of these systems, making the identification of events easier as the signal is stronger. For disturbances that exhibit significant movement in the meridional direction, this technique does not work well due to the mixing of phases. Also, for those events that display high variability within their respective category, the composites do not provide a good representation of their characteristics.

An Eulerian view of the environmental conditions and its evolution can be gathered from the horizontal composite of the fields at different time lags from the initiation date. This is done by plotting the relative vorticity anomaly at 850 hPa, the horizontal wind and surface pressure anomaly. It helps in distinguishing the large-scale features associated with each event category.

As LPS are propagating systems, their properties can be represented better in a Lagrangian framework, by tracking their positions. For the next part of the analysis, the initiation date, location and track are identified using an automated algorithm, with the archive of low initiation dates as reference. A low pressure system is identified as a centre of maximum vorticity at 850 hPa, which has pressure anomaly with magnitudes greater than 2 hPa within 5^0 of the vortex centre (criteria adopted by IMD for classification of a disturbance as a LPS, shown in Table 2). A box is defined in the Bay of Bengal region (15^0 to 25^0 N, 85^0 to 95^0 E) and the location of maximum relative vorticity anomaly at 850 hPa on the grid is identified. If surface pressure anomaly (calculated from the 21-day running mean) falls below -2 hPa within a 5^0 box around the vortex centre, then it is classified as a low.

Calculating anomaly from 21-day running mean helps to filter out the lower frequency anomaly patterns corresponding to time scales greater than 21 days. In a way, the effect of intraseasonal oscillations (30-60 day mode) is reduced. The choice of box may not be able to capture all the cases of initiation due to the variability in the location of low pressure initiation.

Table 2: Classification of monsoon LPS into low, depression, deep depression or stronger using sea level pressure anomaly and maxima of horizontal wind at the surface based on IMD criteria. Amplitudes of sea level pressure anomaly are negative (Hurley and Boos, 2014).

	Monsoon Low	**Monsoon Depression**	**Deep depressions and stronger**
Mean sea-level pressure anomaly	>= 2 hPa	>= 4 hPa and <= 10 hPa	>= 10 hPa
Maximum of horizontal wind speed at the surface		>= 8.5 ms^{-1} and <= 13.5 ms^{-1}	>= 13.5 ms^{-1}

The algorithm applied for tracking a LPS is as follows:

1. Identify the location of maximum relative vorticity anomaly at 850 hPa on the grid;
2. Calculate the pressure anomaly in a 5^0 box around the vortex centre;
3. If this falls below -2 hPa (at least once in 4 time steps), then the vortex centre is identified as the centre of the LPS;
4. The next location is identified by repeating step 1 in a 3^0 box around the vortex centre of the current iteration;
5. Steps 2 through 4 are repeated until the pressure anomaly constraint is not satisfied.

After tracking, the horizontal and vertical composites of the associated dynamic and thermodynamic fields are constructed by averaging across time steps and across events. Although each event differs from another, compositing helps to bring out the common features in each category and also aids in comparison. An error in the identification of date and location of initiation could lead to tracking of events that are not necessarily part of the monsoon LPS.

The errors contributed by the spatial resolution of data is reduced to a considerable degree by applying the tracking procedure on both 1^0 x 1^0 and 0.75^0 x 0.75^0 grids. Comparison of tracks show that they agree reasonably well.

3. RESULTS

3.1. Statistics of low pressure system initiation

On examining the time-longitude distribution of relative vorticity anomaly at 850 hPa for 39 years (1979-2017), 256 low pressure initiation events over Bay of Bengal were identified. Of the total, 173 or 68% were found to form in-situ and 83 or 32% by downstream amplification. Among the in-situ initiation cases, 49 (19%) were non-propagating, 10 (4%) were eastward propagating and 114 (45%) were westward propagating.

The spatial distribution of the locations of low initiation for 39 years is shown in Fig. 1. Low pressure initiation by downstream processes seems to be preferentially located near the head of Bay of Bengal and western coast of Myanmar as is seen in the clustering of the green markers in the region. Their initiation latitude is always above 15^0 N. The in-situ cases (all of the three categories) seem to be more randomly distributed, with a greater number of them initiated over ocean compared to land.

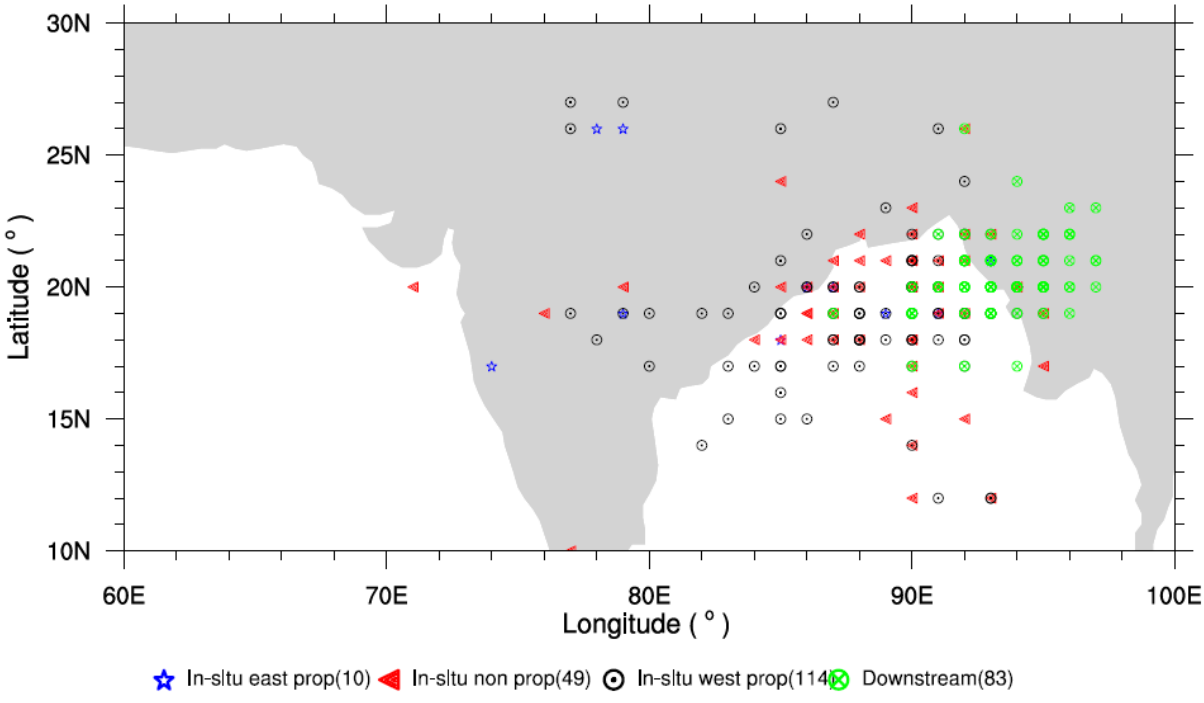

Figure 1: Locations of initiation of low pressure systems during monsoon for 1979 to 2019. Green circles represent downstream events, black circles represent in-situ westward propagating events, red triangles represent in-situ non-propagating events and blue star represents in-situ eastward propagating events.

Most of the lows that we examined intensified when it was located over ocean and decayed upon entering land, as it is cut off from the moisture supply. A few cases of lows that were able to intensify over land were also identified.

Different processes were active during different periods of time. In the month of June, the downstream processes did not have much role in the initiation of lows (Fig. 2), as most of the lows were initiated in-situ. Intensity of lows initiated in June was found to be comparatively lower. A small number of cases were initiated at low latitudes (with lower planetary vorticity) also having lower intensities.

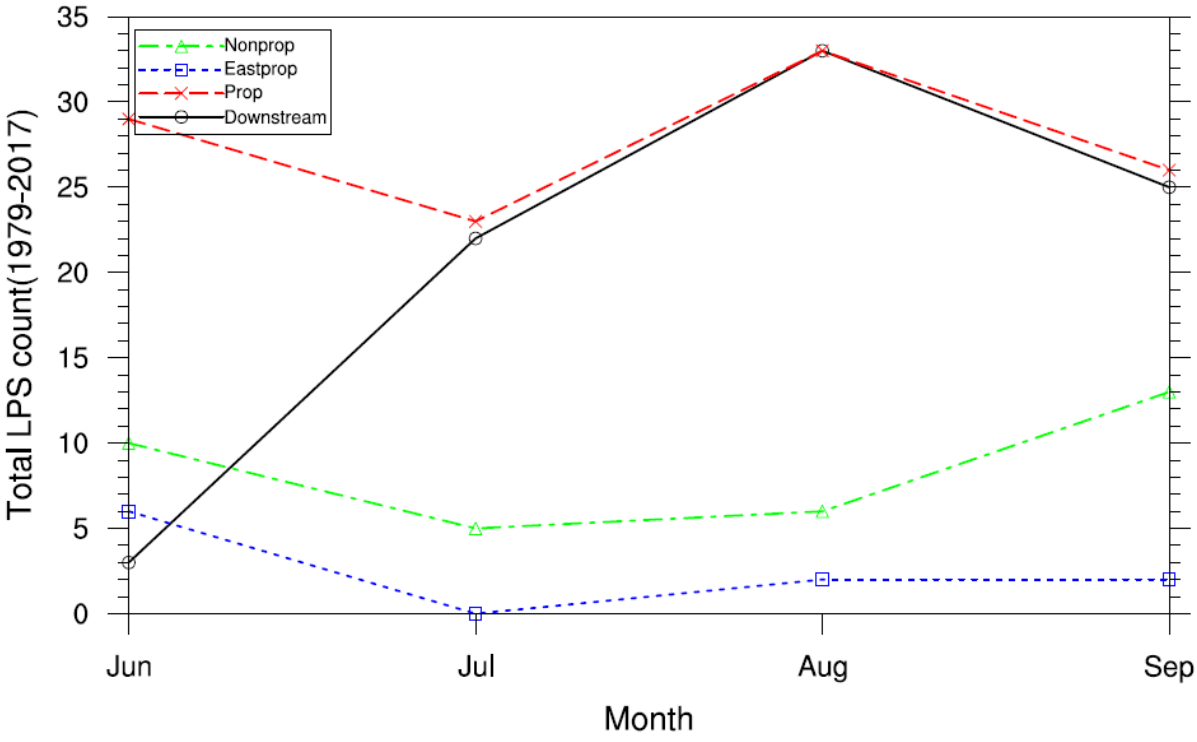

Figure 2: Monthly variation in low pressure initiation for 1979 to 2017 over Bay of Bengal. Green, blue, red and black lines represent in-situ non propagating events, in-situ eastward propagating events, in-situ westward propagating events and downstream events respectively.

Typhoons occurring in the Pacific or their remnants could be traced to be the precursors for low pressure initiation in the downstream cases (Saha et al., 1981). These are seen as high amplitude propagating patterns in the latitude-longitude distribution of relative vorticity anomaly. The number of lows initiated by downstream processes are high during the months of August and September, the peak season of

typhoons in western Pacific (Joint Typhoon Warning Centre, Annual Tropical Cyclone Report, 2017), and considerably lower during June when the vertical wind shear is high.

In Fig. 3, we examine the composite time-longitude plot to study the propagation characteristics that are common within each category. The time-longitude plot shows the zonal motion of the system with time when averaging is carried out across a suitable latitude range. The zonal motion is identified by the presence of a tilt in the plots. The time runs from 4 days prior to the initiation date to 4 days after.

From the composite plot, the influence of propagating cyclonic disturbances from the Pacific (indicated by the red shading), with westward slope corresponding to westward propagation is clearly seen in the downstream case (see Fig. 3a). Positive anomaly values occur in the western Pacific a few days prior to its occurrence in the Bay of Bengal and propagate westward. This pattern is absent in the in-situ propagating case, with negative values seen in the western Pacific close to the initiation date (Fig. 3b).

The downstream composite is centred at 88^0 E, with greater amplitude and slower speed of phase propagation (3 - 4 m s^{-1}) compared to the *in-situ* propagating (5 m s^{-1}) composite. This could be due to greater variability in the location and phase speed of in-situ propagating events (see Fig. 1), which causes mixing of phases, leading to a reduction in amplitude. The in-situ westward propagating composite is centred at 90^0 E and the positive anomaly values associated with the system are confined to longitudes west of Bay of Bengal. As there is no observable slope, Fig. 3c correspond to non-propagating events. Due to the lesser number of events over which averaging is carried out in the eastward propagating composite, the amplitudes appear to be greater.

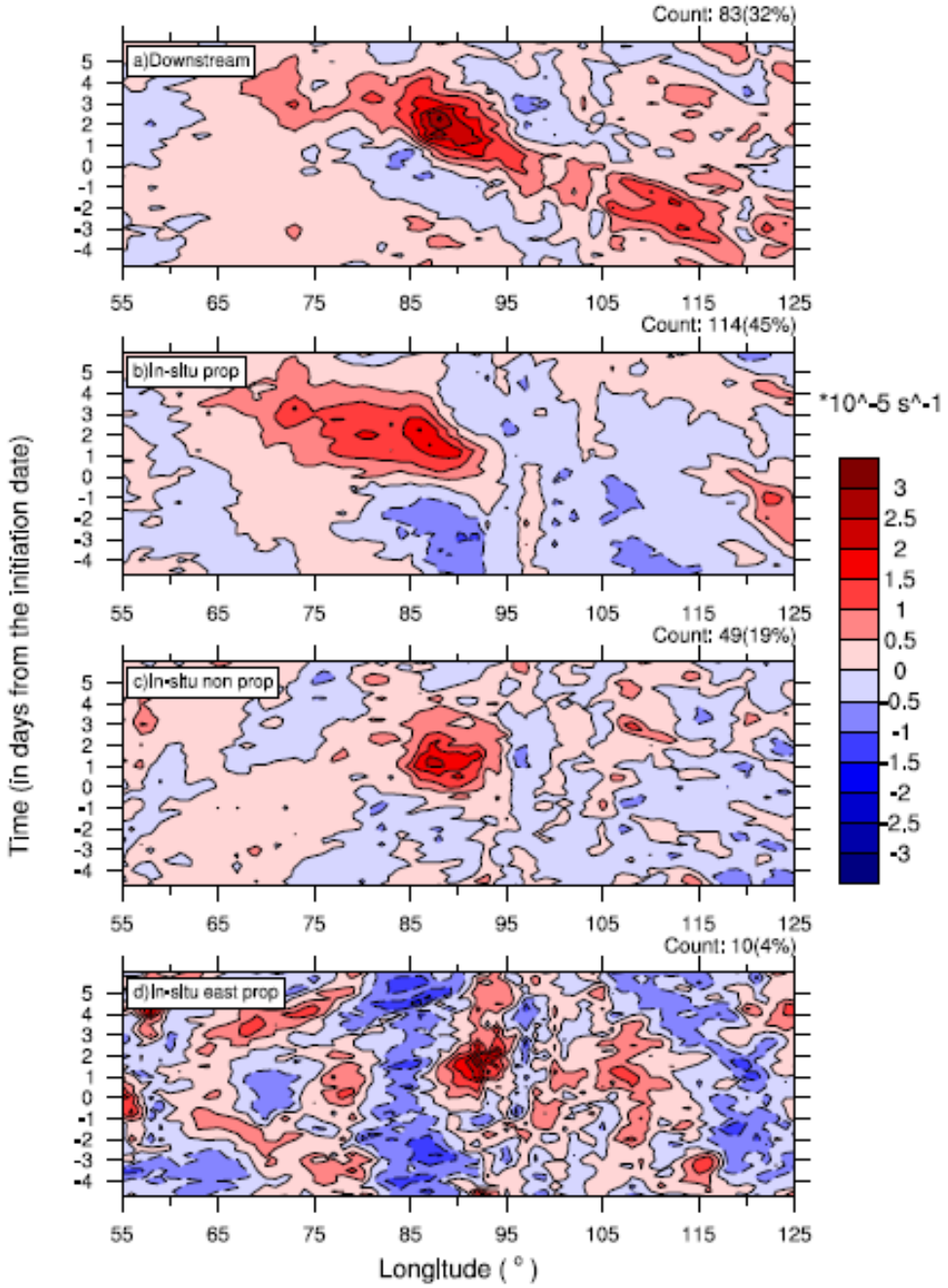

Figure 3: Composite plots of relative vorticity anomaly (in 10^{-5} s^{-1}) at 850 hPa for (a) downstream (b) in-situ propagating (c) in-situ non-propagating and (d) in-situ eastward propagating events. Positive values (red) represent cyclonic and negative values (blue, dashed contours) represent anticyclonic vorticity. Values indicated as count in the top-right corner correspond to the number of events of each type with their respective percentages (of the total) enclosed in brackets.

The mean track of *in-situ* propagating and downstream events and their most probable paths are shown in Fig. 4. For calculating the mean track, the events that lasted for 4.5 days (or 18 time steps) were chosen and their positions were averaged across. In

the in-situ propagating case, 62 events were averaged and for the downstream case, 50 events were averaged.

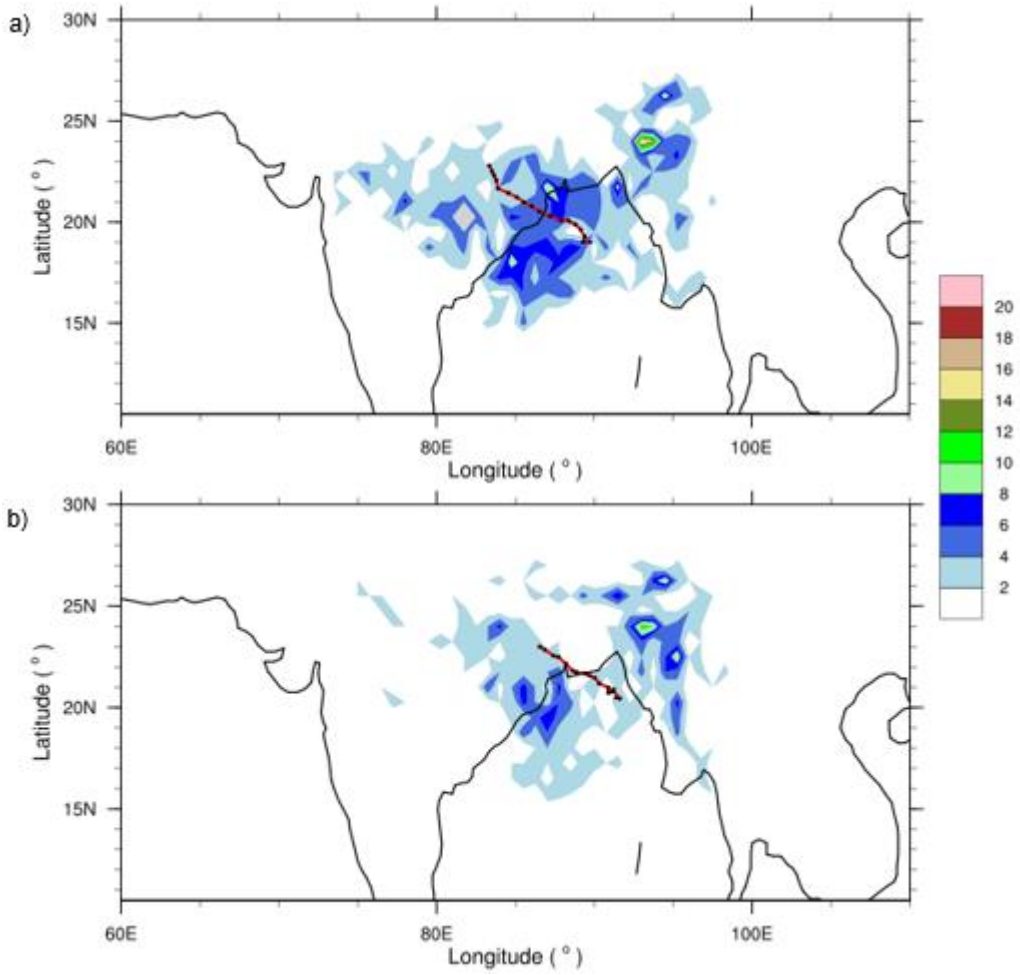

Figure 4: Mean track (red line) of (a) *in-situ* westward propagating and (b) downstream events. Black dot represents the position for every 6 hours (one time step). Shading represents the number of LPS that passed through a particular point.

Both categories of events display a mean north-westward movement. The track of *in-situ* westward propagating events exhibit greater zonal (westward) and meridional (northward) motion compared to downstream events within the same time span, indicating a higher propagation speed (as seen in Fig. 3). Fig. 4b indicates the two distinct paths that downstream events prefer to follow. The region to the west of the head Bay is favoured by lows initiated *in*-situ. We see that the mean track represents the most probable path of LPS better for events initiated *in-situ* compared to downstream events. The initiation location of downstream events is situated to the east of head Bay (shown in Fig. 1). As the tracks are created by an objective algorithm,

the visibly different propagation character of the two kinds of events (in-situ westward propagating and downstream) observed in the previous figures are verified.

Fig. 5 shows the interannual variability in low initiation. The downstream events show a decreasing trend whereas the in-situ events show a slightly increasing trend. They are weakly anti-correlated with a correlation coefficient of -0.24. On the whole, a decreasing trend is seen in the total number of lows initiated in the Bay of Bengal region. Downstream processes attribute some amount of predictability to LPS initiation in Bay of Bengal (Saha et al., 1981). The initiation of lows become more unpredictable as the *in-situ* processes, which show greater randomness in the initiation location and propagation characteristics become increasingly important.

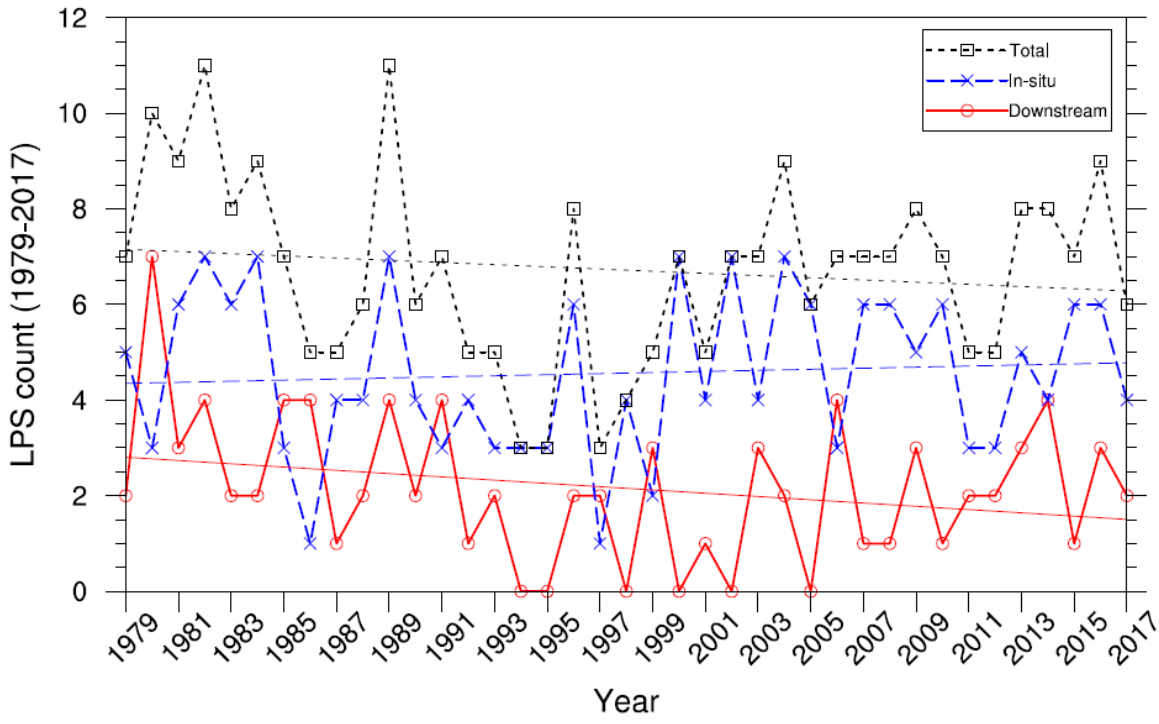

Figure 5: Inter annual variability in LPS initiation. Blue lines represent *in-situ* events, red lines represent downstream events and the black dotted lines represent the total number of events. The lines drawn without markers indicate the trend in the time series.

We see that *in-situ* westward propagating and downstream events contribute to the largest fraction of lows over Bay of Bengal during the period of the study. In the next section, we focus specifically on these two types of events.

3.2. Composite structure

In this section, we try to study the common features that emerge from the compositing procedure. Both Eulerian and Lagrangian views of the systems are presented.

3.2.1. In-situ propagating composite

The lifecycle composite of each type of event is created by compositing relative vorticity anomaly at 850 hPa, surface pressure anomaly and horizontal winds at 1000 hPa. The plots are made for the *in-situ* propagating events before, during and after the initiation date as illustrated in Fig. 6. This gives an indication of the large-scale features present near the initiation period and how these evolve in time.

The winds are southwesterly and the vorticity values are negative at the head Bay four days prior to the initiation date (Fig. 6a). At this time positive vorticity anomaly values are present north of 23^0 N at longitudes of Bay of Bengal. After 2 days, this region of positive vorticity shifts downward and slightly intensifies as seen in Fig. 6b. On the initiation date, vorticity has further intensified and it attains a well-marked structure, as observed in the presence of closed pressure contours around the vortex centred at 23^0 N and 85^0 E (Fig. 6c). In the following days, the system moves westward across land and suffers a reduction in its intensity (Fig. 6d, 6e). A broad region of positive vorticity is observed to move along with the disturbance.

Since these are propagating systems, their behaviour is best studied in a frame of reference which moves along with them. By using the objective criteria specified by IMD, identifying a LPS as a vortex centre with pressure anomalies associated with them, a tracking algorithm (described in chapter 2) is developed to detect and follow these systems. Both dynamic and thermodynamic field variables are composited across time steps and events in a 3^0 box about the vortex centre. A Lagrangian view of the system is provided by this compositing procedure. It averages across the lifecycle of the LPS and does not differentiate between the different types, i.e., low, depression, deep depression. A total of 85 *in-situ* propagating events are composited to obtain the structures described below.

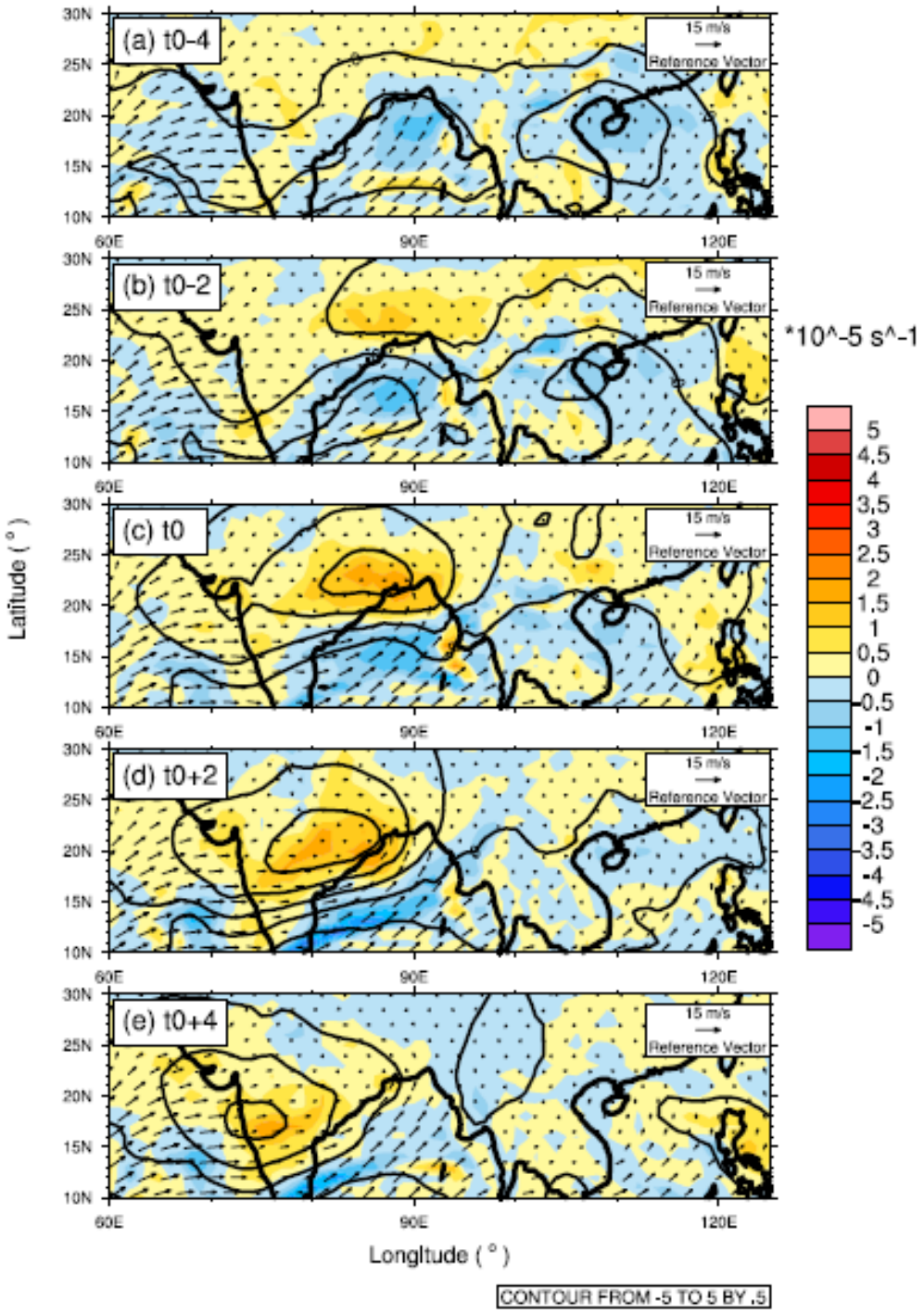

Figure 6: Lifecycle composite of *in-situ* propagating events for (a) t_0 - 4 (b) t_0 - 2 (c) t_0 (d) t_0 + 2 and (e) t_0 + 4, where t_0 is the initiation date. Shading denotes vorticity anomaly (in 10^{-5} s^{-1}) at 850 hPa, black contours denote surface pressure anomaly (in hPa) and the arrows represent the horizontal winds (in m s^{-1}), both zonal and meridional at 1000 hPa. Reference wind vector has magnitude of 15 m s^{-1}.

The horizontal and vertical structure of the relative vorticity anomaly composite is depicted in Fig. 7. As each case differs in the location of initiation, the composite

structures represent the distribution of quantities with respect to the centre of the LPS. The vertical profile of relative vorticity (Fig. 7a) shows a maximum of 10 x 10^{-5} s^{-1} at approximately 875 hPa. The highest values (> 5 x 10^{-5} s^{-1}) are confined between 650 to 900 hPa and maintains an upright structure. The low values present near the surface may be due to the dissipative effects of friction. Maximum vorticity values (5 x 10^{-5} s^{-1}) at 850 hPa are observed at the centre with cyclonic winds and a distribution that is nearly symmetric about it (Fig. 7b). Positive values are maintained within the 3^0 box around the centre.

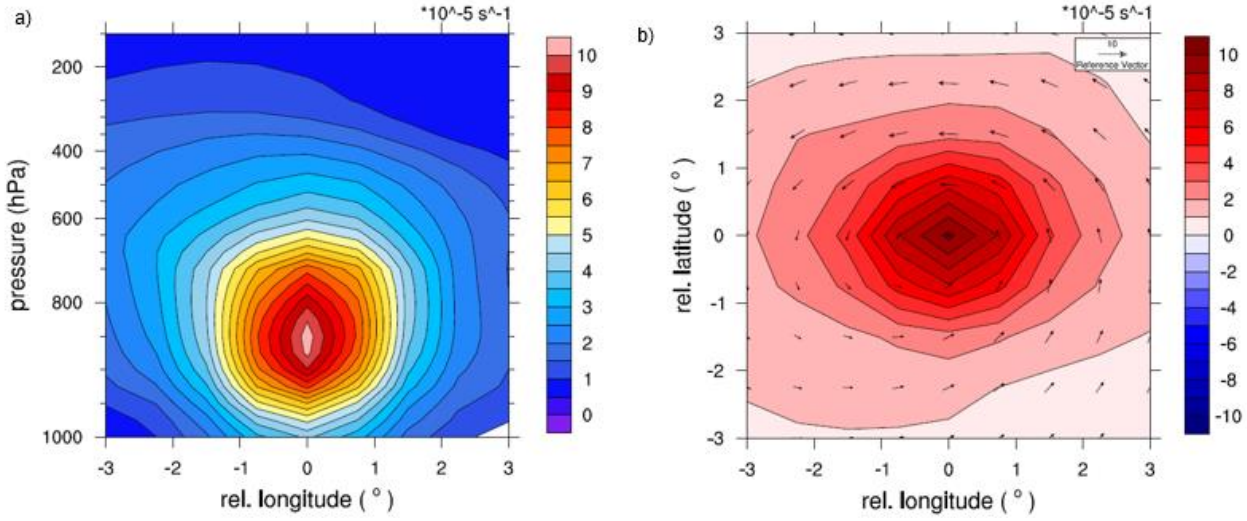

Figure 7: Relative vorticity anomaly composite (a) zonal cross section of vertical profile centred at the latitude of low (b) horizontal structure at 850 hPa with wind vectors. Shading denotes vorticity anomaly (in 10^{-5} s^{-1}), arrows represent the horizontal wind anomaly (in m s^{-}1) at 850 hPa. Reference wind vector has magnitude of 10 m s^{-1}. Negative relative longitude values are used to refer to regions to the west and negative relative latitude values correspond to the regions south of the centre.

The profile of total wind is plotted in Fig. 8 which helps to study the properties of the mean state in which these systems form. Positive values represent westerlies and negative values denote easterlies for the zonal wind profile. The highest values of westerlies are observed at 850 hPa, to the south of the vortex centre (Fig. 8a). The winds are mostly westerly to the south and easterly to the north, displaying significant horizontal shear in the mean wind. Vertical shear is high in the region where a transition occurs from westerlies to easterlies at around 400 hPa. Strong easterlies dominate the upper levels.

For the meridional wind profile, negative values represent northerly winds. The winds are mostly northerly to the west and southerly to the east, showing horizontal shear in the mean meridional wind (Fig. 8b).

Maximum southerly winds are observed at 850 hPa to the east of the vortex centre. Compared to the zonal winds, the meridional winds are weaker.

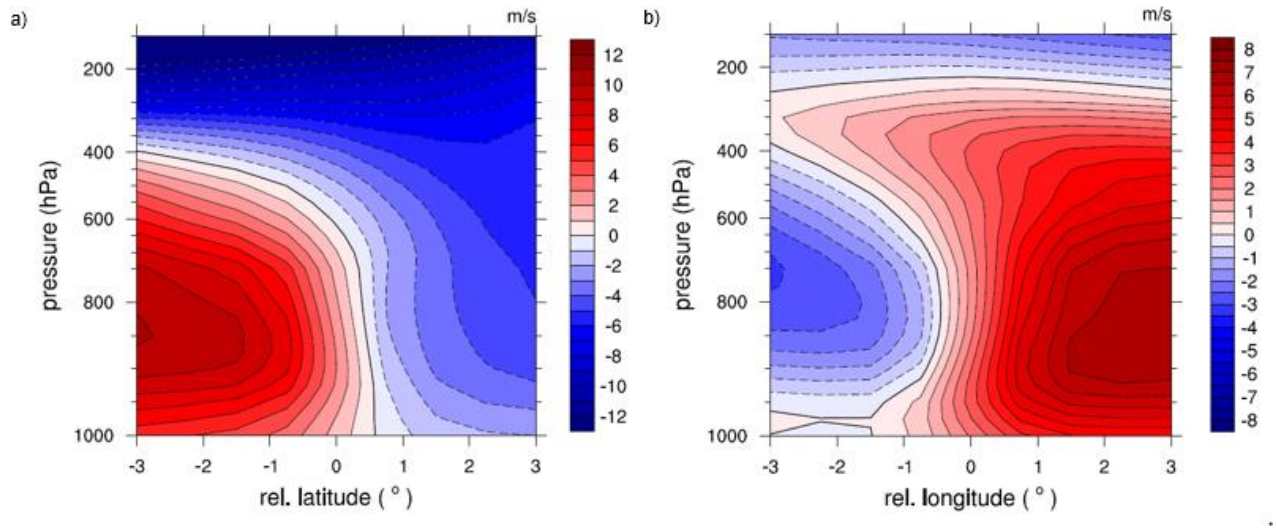

Figure 8: (a) Meridional cross section of zonal velocity profile (b) Zonal cross section of meridional velocity. Dashed contours indicate negative values. Units are in m s^{-1}.

The vertical profiles of anomalies of vertical pressure velocity, potential vorticity, temperature and specific humidity are shown in Fig. 9. Pressure velocity profiles are indicators of the convergence patterns at each of the pressure levels. Its profile shows maximum ascent occurring at 800 hPa (Fig. 9a) at the centre of the system. There is a westward tilt with height in the profile that agrees with the behaviour of the system observed in previous studies (Hunt et al., 2016).

Potential vorticity is a parameter that combines both dynamic and thermodynamic fields. The vertical structure (Fig. 9b) shows positive values extending from near the surface to upper troposphere with two maxima, one at 850 hPa and a comparatively lower value at 500 hPa. The profile remains upright with appreciably larger amplitudes (>2.5 x 10^{-7} K m^2 kg^{-1} s^{-1}) confined between 400 and 900 hPa. The vertical structure of PV noted in the present study is different from those reported in previous studies (Boos et al., 2014, Hunt et al., 2016) that treat MDs as top-heavy columns of PV, with maxima in the mid troposphere.

The temperature anomaly profile (Fig. 9c) is representative of the warm over cold core thermal structure. The greatest cooling (nearly 1.25 K) occurs near the surface, to the west of the centre in agreement with the observations. Highest amplitude of warming also occurs to the west of the centre at 400 hPa. Fig. 9d shows the greatest moistening in the middle levels at nearly 750 hPa also to the west of the centre.

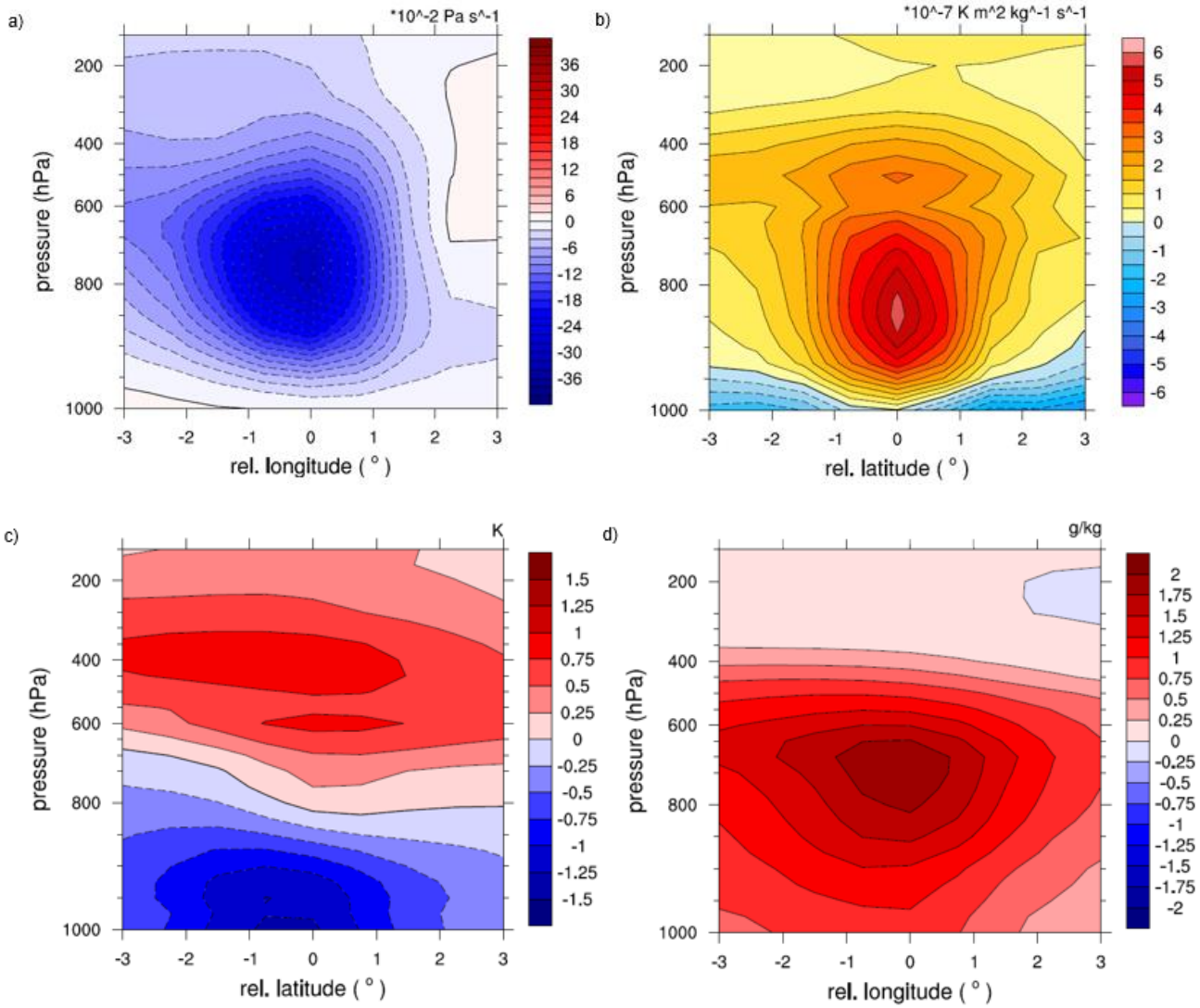

Figure 9: (a) Zonal cross section of pressure velocity anomaly profile (in 10^{-2} Pa s^{-1}) (b) Meridional cross section of Potential Vorticity anomaly profile (in 10^{-7} K m^2 kg^{-1} s^{-1}) (c) Meridional cross section of temperature anomaly profile (in K) (d) zonal cross section of specific humidity anomaly profile (in g/kg). Dashed contours indicate negative values. For (a), dashed contours (blue shading) represent ascent.

These systems transport moisture upwards from the lower levels causing evaporative cooling and subsequently release latent heat of condensation, warming the middle levels.

3.2.2. Downstream composite

The Eulerian composite of downstream events before, during and after the low pressure initiation date is shown in Fig. 10. The presence of a precursor disturbance in the Pacific located at 120E can be seen in Fig. 10a, reflected in the cyclonic vorticity values and closed pressure contours, four days prior to initiation. It propagates westward over land (Fig. 10b) maintaining its structure and reaches Bay of Bengal region on the initiation date (Fig. 10c). It intensifies over the Bay two days later (Fig. 10d), seen in the increase in amplitude of cyclonic vorticity and an increase in the number of closed pressure contours about this vortex centre. Afterwards, the low centre moves westwards and decays upon entering land (Fig. 10e).

Four days prior to initiation, another cyclonic disturbance is present in the Bay of Bengal region, which then proceeds to propagate westward. Multiple lows can be initiated in succession by downstream generation.

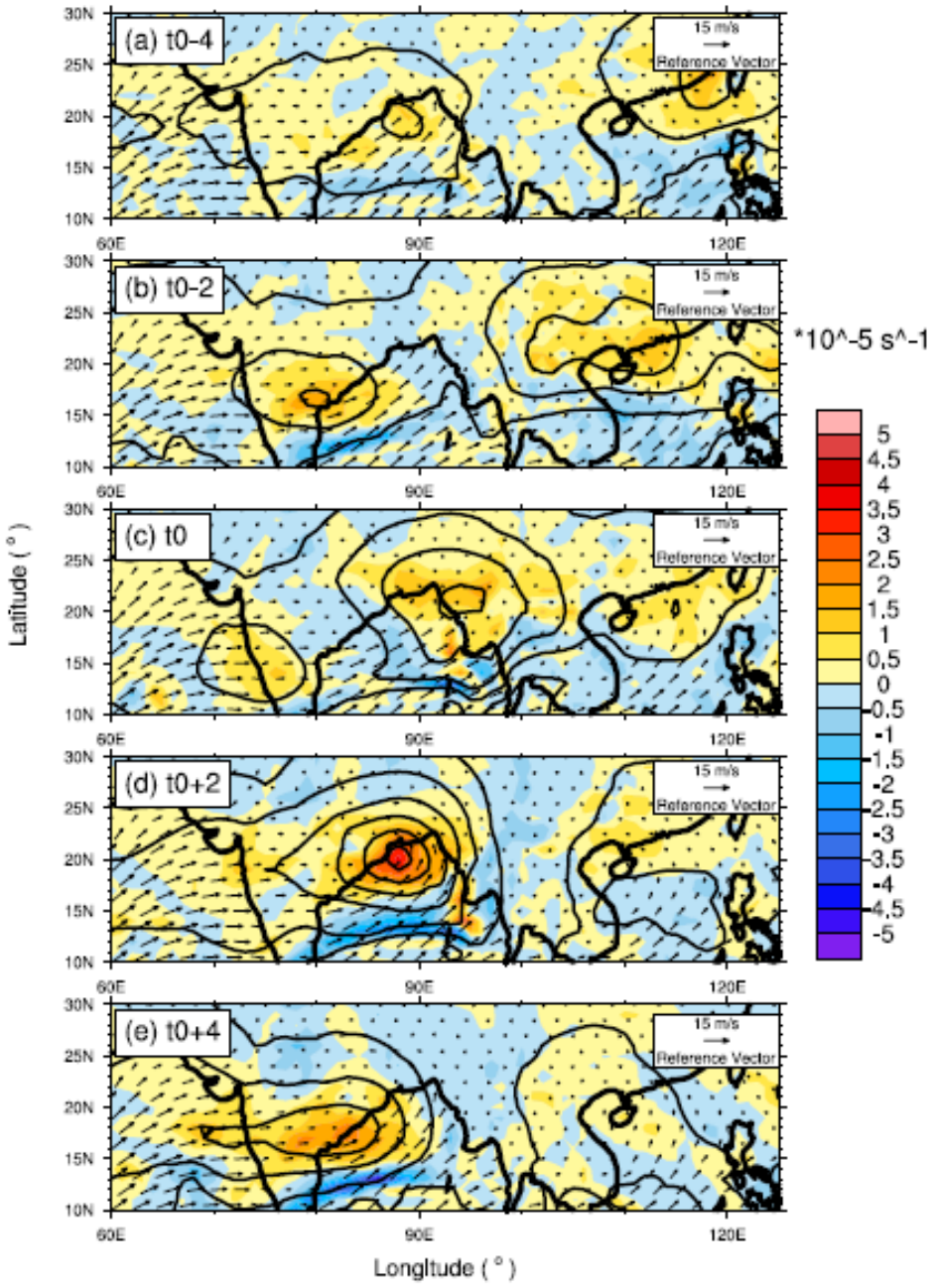

Figure 10: Lifecycle composite of downstream events for (a) t_0 - 4 (b) t_0 - 2 (c) t_0 (d) t_0 + 2 and (e) t_0 + 4, where t_0 is the initiation date. Shading denotes vorticity anomaly (in 10^{-5} s^{-1}) at 850 hPa, black contours denote surface pressure anomaly and the arrows represent the horizontal winds (in m s^{-1}), both zonal and meridional, at 1000 hPa. Reference wind vector has magnitude of 15 m s^{-1}.

Fig. 11 represents the relative vorticity anomaly composite of the zonal cross section of vertical profile centred at the latitude of low initiation and horizontal structure at 850 hPa along with wind vectors. For calculating the composite structure, 63 cases of downstream generated events are composited.

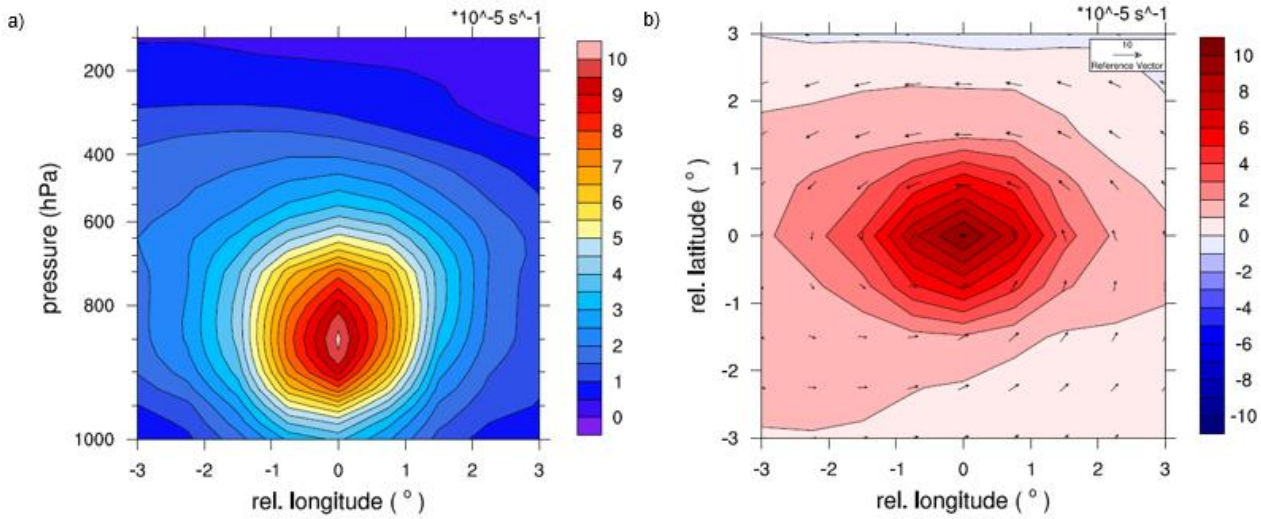

Figure 11: Relative vorticity anomaly composite (a) zonal cross section of vertical profile centred at the latitude of low (b) horizontal structure at 850 hPa with wind vectors. Shading denotes vorticity anomaly (in 10^{-5} s^{-1}), arrows represent the horizontal wind (in m s^{-1}) at 850 hPa. Reference vector has magnitude of 10 m s^{-1}.

The vertical profile of relative vorticity (Fig. 11a) shows a maximum of 10 x 10^{-5} s^{-1} at approximately 850 hPa. The highest values (> 5 x 10^{-5} s^{-1}) are confined between 650 to 900 hPa and maintains an upright structure. Maximum values (5 x 10^{-5} s^{-1}) are observed at the centre with cyclonic winds and a distribution that is nearly symmetric about it (Fig. 11b). Positive values are maintained within the 3^0 box.

The vertical composite profile of the mean zonal and meridional velocity is presented in Fig. 12. The highest values of westerly winds (positive values) are observed at 850 hPa, to the south of the vortex centre (Fig. 12a). The winds are mostly westerly to the south and easterly to the north, showing significant horizontal shear in the mean wind. Vertical shear is present in the region where westerlies transition to easterlies at around 450 hPa. Strong easterlies dominate the upper levels.

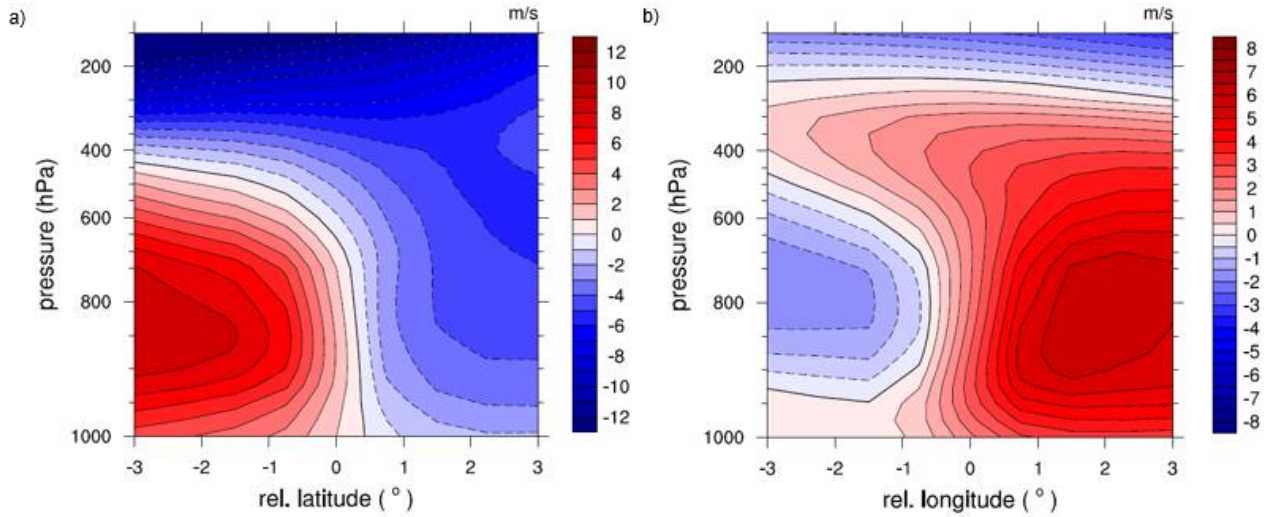

Figure 12: (a) Meridional cross section of zonal velocity profile (b) Zonal cross section of meridional velocity. Dashed contours indicate negative values. Units are in m s^{-1}.

The winds are mostly northerly (negative, dashed contours) to the west and southerly to the east, showing horizontal shear in the mean meridional wind (Fig. 12b). Maximum southerly winds are observed at 850 hPa to the east of the vortex centre.

Fig. 13 illustrates the profiles of anomalies of pressure velocity, potential vorticity, temperature and specific humidity. Negative pressure velocity values representing ascent are highest at 800 hPa, located at the centre (Fig. 13a). It also displays a westward tilt with height in the profile.

The vertical structure of potential vorticity (Fig. 13b) shows positive values extending from near the surface to upper troposphere with two maxima, one at 850 hPa and another comparatively lower value at 500 hPa. The profile remains upright with appreciably larger amplitudes (>2.5 x 10^{-7} K m^2 kg^{-1} s^{-1}) confined between 400 and 900 hPa.

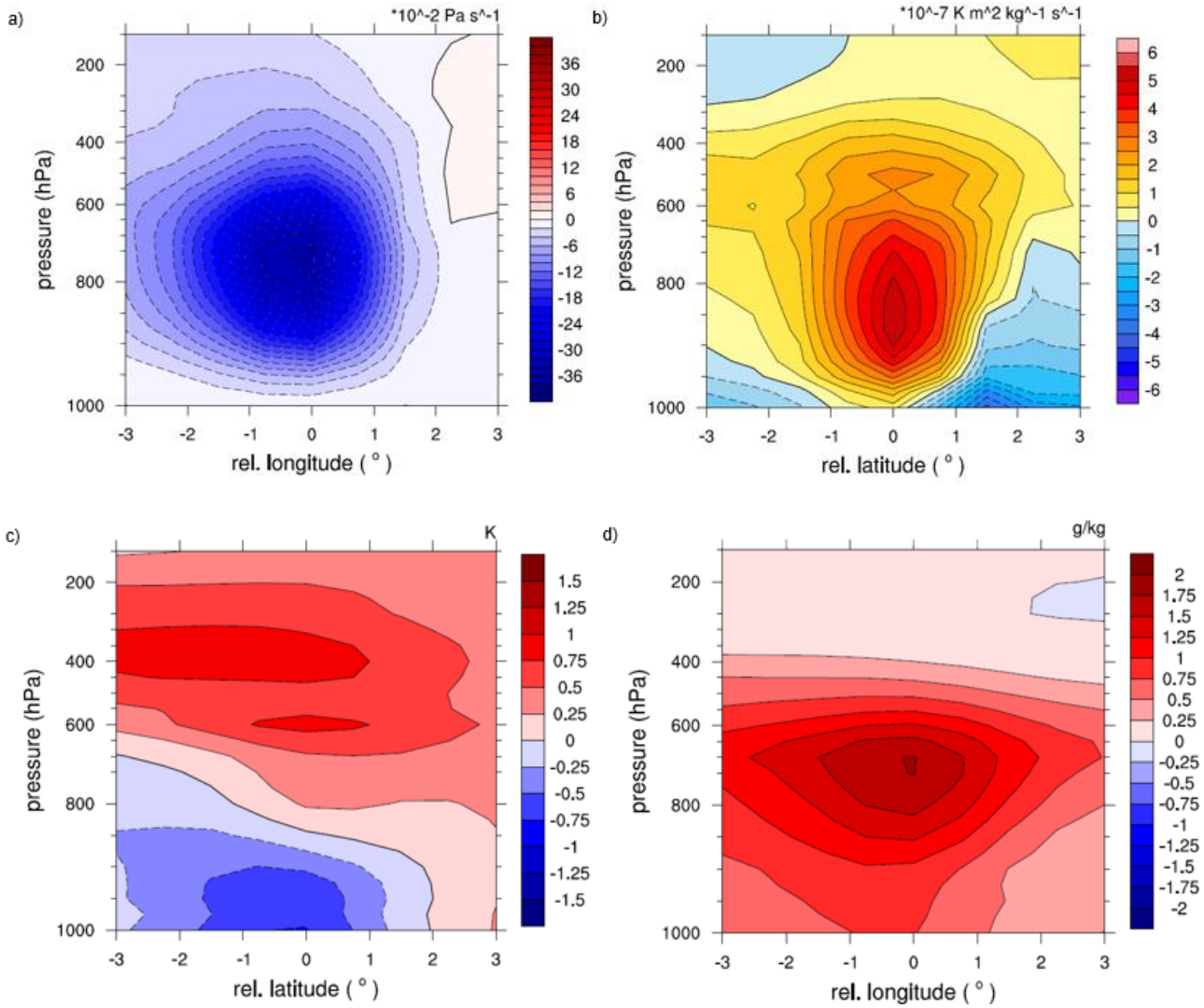

Figure 13: (a) Zonal cross section of pressure velocity anomaly profile (in 10^{-2} Pa s^{-1}) (b) Meridional cross section of Potential Vorticity anomaly profile (in 10^{-7} K m^2 kg^{-1} s^{-1}) (c) Meridional cross section of temperature anomaly profile (in K) (d) zonal cross section of specific humidity anomaly profile (in g/kg). Dashed contours indicate negative values. For (a), dashed contours (blue shading) represent ascent.

The temperature anomaly profile (Fig. 13c) indicates a warm over cold core thermal structure. The greatest cooling occurs near the surface, to the west of the centre while the highest amplitudes of warming are found to occur to the west of the centre at 400 hPa. Moistening is the greatest in the middle levels at nearly 700 hPa, also to the west of the centre (Fig. 13d).

4. DISCUSSION

Low pressure systems, with an average occurrence of 14 per year, are the agents responsible for the organisation of convection and the subsequent distribution of a large fraction of rainfall over central India. They initiate *in-situ* over Bay of Bengal or through the influence of propagating cyclonic disturbances from the western Pacific. Initiation of lows over Bay of Bengal is found to be influenced mainly by *in-situ* processes (68%) in comparison to downstream processes (32%). The statistics obtained is different from the previous studies by Krishnamurti et al. (1977) or Saha et al. (1981), where the majority of low initiation is shown to occur by downstream amplification.

The classification of an event as downstream generated may be done objectively by calculating the cyclonic vorticity flux across the longitude corresponding to Bay of Bengal. Using the wavenumber-frequency relation of wave disturbances from the western Pacific, their group velocity may be determined and the trajectory of energy propagation into the Bay mapped out.

The composite structures provide a way of comparing *in-situ* propagating and downstream cases. The lifecycle composite (Eulerian or field view) in the downstream case shows a cyclonic disturbance propagating across Pacific into Bay of Bengal. Such a kind of organised structure in both vorticity and pressure fields originating in the Pacific is not detected in the *in-situ* case.

A Lagrangian view of the horizontal and vertical structures of the dynamic and thermodynamic fields are very similar in the two categories. The relative vorticity profile has a maximum in the lower troposphere, away from the surface, has an upright structure and is contained below the mid troposphere. It is embedded in a background of strong westerlies (see Figs. 8 and 12) that are present in the lower levels and propagate north-westward against the mean flow. Both zonal and meridional mean winds have significant horizontal shear which can modify the cyclonic vorticity of the environment. The distribution of ascent (negative values of pressure velocity) shows a westward tilt with height consistent with the observations.

The temperature profile is characterised by a warm core over cold core structure, with evaporation cooling the lower levels and release of latent heat of condensation

warming the upper levels while transporting moisture from the lower levels into the middle levels. The thermal stratification of the system is stable with a maximum around 850 hPa. This is reflected in the PV profile (a product of relative vorticity and stratification) which peaks at 850 hPa at the vortex centre.

In a conditionally unstable tropical atmosphere, if any physical process, *in-situ* or downstream, is able to provide an initial kick by lifting moist air parcels, they become positively buoyant and can grow further through the release of latent heat of condensation, tapping into their convectively available potential energy.

In some of the low pressure initiation events, the presence of a vertically propagating signal from the upper troposphere is observed in the distribution of PV anomaly. The growth of a disturbance in this top-down manner is different from the commonly held notion of a bottom-up growth, where the initial disturbance appears in the lower levels and affects the upper levels afterwards. Ortega et al (2017), link the quasi biweekly oscillations occurring in the upper tropospheric to those in the lower troposphere over South Asia during monsoon and show that they are co-evolving.

The dynamic and thermodynamic structure of the two classes (*in-situ* propagating and downstream) of events do not display significant dissimilarity for them to be classified as distinct physical systems. The behaviour of LPS is independent of the physical process responsible for initiation and appears to rely on regional dynamics.

There were some LPS that displayed intensification over land as opposed to the typical decaying behaviour. The soil moisture distribution along the monsoon trough is suggested to play a significant role in modifying the structure and propagation characteristics of MDs (Hunt and Turner, 2017). Large-scale features like the Indian Ocean Dipole, characterised by a dipole structure of SST anomalies in the Indian Ocean, are found to influence the longevity of LPS by affecting the moisture transport (Krishnan et al., 2010). The effect of these processes needs to be explored further. These observations point to the highly non-linear nature of the interactions and the variety of processes involved in the modulation of the behaviour of monsoon LPS.

Lows initiated by *in-situ* processes display greater variability in the initiation date and location. With the number of *in-situ* events on a rise, it will become increasingly difficult to predict their initiation in the future.

5. CONCLUSION

We find that the low pressure systems over Bay of Bengal are mainly initiated *in-situ* (68%) in comparison to downstream initiation (32%), where precursor disturbances are located in the western Pacific. The above statistics are obtained by the analysis of 256 LPS initiation cases identified during the 39 year period from 1979 to 2017. In previous studies, the statistics obtained is different, where downstream amplification is listed as the major contributor to low pressure initiation. The composite analyses show that the dynamic and thermodynamic structure of LPS is independent of the process of initiation and is similar enough for each category to be considered as the same physical system. This indicates the need for models to incorporate the effects of initiation by downstream processes, to account for the western Pacific as a source of vorticity, moisture, without significantly altering the underlying physics. A better understanding of the monsoon LPS is required for a better representation of its effects in climate models. This is important for improving simulations and for making reliable predictions about the monsoon.

Considering monsoon depressions (a category of LPS) as one of the equatorial wave modes, the shallow water equations may be systematically modified to include the effect of various physical processes. The formulation of this influence requires it to be represented in terms of some physical parameter, which is often difficult. It needs to be seen how well the linear theory is able to capture the properties of monsoon depressions and account for the selection of this particular scale in the atmosphere.

REFERENCES

Adames, Á. F., and Y. Ming, 2018: Moisture and moist static energy budgets of south Asian Monsoon Low Pressure Systems in GFDL AM4.0. *Journal of the Atmospheric Sciences*, **75**, 2107–2123, doi:10.1175/jas-d-17-0309.1.

Boos, W. R., J. V. Hurley, and V. S. Murthy, 2014: Adiabatic westward drift of Indian monsoon depressions. *Quarterly Journal of the Royal Meteorological Society*, **141**, 1035–1048, doi:10.1002/qj.2454.

Chatterjee, P., and B. N. Goswami, 2004: Structure, genesis and scale selection of the tropical quasi-biweekly mode. *Quarterly Journal of the Royal Meteorological Society*, **130**, 1171–1194, doi:10.1256/qj.03.133.

Diaz, M., and W. R. Boos, 2019: Barotropic growth of monsoon depressions. *Quarterly Journal of the Royal Meteorological Society*, **145**, 824–844, doi:10.1002/qj.3467.

ERA Interim, Daily. *ECMWF | Public Datasets*. http://apps.ecmwf.int/ datasets/data/ interim-full-daily/levtype=sfc/.

Goswami, B. N., 1987: A mechanism for the west-north-west movement of monsoon depressions. *Nature*, **326**, 376–378, doi:10.1038/326376a0.

Hunt, K. M. R., and A. G. Turner, 2017: The effect of soil moisture perturbations on Indian monsoon depressions in a numerical weather prediction model. *Journal of Climate*, **30**, 8811–8823, doi:10.1175/jcli-d-16-0733.1.

Hunt, K. M. R., A. G. Turner, P. M. Inness, D. E. Parker, and R. C. Levine, 2016: On the structure and dynamics of Indian monsoon depressions. *Monthly Weather Review*, **144**, 3391–3416, doi:10.1175/mwr-d-15-0138.1.

Hunt, K. M. R., and D. J. Parker, 2016: The movement of Indian monsoon depressions by interaction with image vortices near the Himalayan wall. *Quarterly Journal of the Royal Meteorological Society*, **142**, 2224–2229, doi:10.1002/qj.2812.

Hurley, J. V., and W. R. Boos, 2014: A global climatology of monsoon low-pressure systems. *Quarterly Journal of the Royal Meteorological Society*, **141**, 1049–1064, doi:10.1002/qj.2447.

IMD - Seismological Services. http://www.imd.gov.in/pages/monsoon_main.php.

JTWC - https://www.metoc.navy.mil/jtwc/products/atcr/2017atcr.pdf.

Kiladis, G. N., M. C. Wheeler, P. T. Haertel, K. H. Straub, and P. E. Roundy, 2009: Convectively coupled equatorial waves. *Reviews of Geophysics*, **47**, doi:10.1029/2008rg000266.

Krishnamurti, T. N., J. Molinari, H.-L. Pan, and V. Wong, 1977: Downstream Amplification and Formation of Monsoon Disturbances. *Monthly Weather Review*, **105**, 1281–1297, doi:10.1175/1520-0493(1977)105<1281:daafom>2.0.co;2.

Krishnan, R., D. C. Ayantika, V. Kumar, and S. Pokhrel, 2010: The long-lived monsoon depressions of 2006 and their linkage with the Indian Ocean Dipole. *International Journal of Climatology*, **31**, 1334–1352, doi:10.1002/joc.2156.

Ortega, S., P. J. Webster, V. Toma, and H.-R. Chang, 2017: Quasi-biweekly oscillations of the South Asian monsoon and its co-evolution in the upper and lower troposphere. *Climate Dynamics*, **49**, 3159–3174, doi:10.1007/s00382-016-3503-y.

Praveen, V., S. Sandeep, and R. S. Ajayamohan, 2015: On the relationship between mean monsoon precipitation and low pressure systems in climate model simulations. *Journal of Climate*, **28**, 5305–5324, doi:10.1175/jcli-d-14-00415.1.

Roundy, P. E., and W. M. Frank, 2004: A climatology of waves in the equatorial region. *Journal of the Atmospheric Sciences*, **61**, 2105–2132, doi:10.1175/1520-0469(2004)061<2105:acowit>2.0.co;2.

Saha, K., F. Sanders, and J. Shukla, 1981: Westward propagating predecessors of monsoon depressions. *Monthly Weather Review*, **109**, 330–343, doi:10.1175/1520-0493(1981)109<0330:wppomd>2.0.co;2.

Sanders, F., 1984: Quasi-geostrophic diagnosis of the monsoon depression of 5–8 July 1979. *Journal of the Atmospheric Sciences*, **41**, 538–552, doi:10.1175/1520-0469(1984)041<0538:qgdotm>2.0.co;2.

Shukla, J., 1976: On the dynamics of monsoon disturbances. D.Sc thesis, MIT, 178 pp

Shukla, J., 1978: Barotropic-baroclinic instability of mean zonal wind during summer monsoon. *Monsoon Dynamics*, 1449–1461, doi:10.1007/978-3-0348-5759-8_18.

Sikka, D. R., 1978: Some aspects of the life history, structure and movement of monsoon depressions. *Monsoon Dynamics*, 1501–1529, doi:10.1007/978-3-0348-5759-8_21.

Sikka, D. R., 2006: *A study on the monsoon low pressure systems over the Indian Region and their relationship with drought and excess monsoon seasonal rainfall*. Center for Ocean-Land-Atmosphere Studies, Center for the Application of Research on the Environment.

Webster, P., and J. Fasullo, 2003: MONSOON | Dynamical Theory. *Encyclopedia of Atmospheric Sciences*, 1370–1386, doi:10.1016/b0-12-227090-8/00236-0.

Williams, E., and N. Renno, 1993: An analysis of the conditional instability of the tropical atmosphere. *Monthly Weather Review*, **121**, 21–36, doi:10.1175/1520-0493(1993)121<0021:aaotci>2.0.co;2.

Yoon, J.-H., and T.-C. Chen, 2005: Water vapor budget of the Indian monsoon depression. *Tellus A*, **57**, 770–782, doi:10.1111/j.1600-0870.2005.00145.x.